JOURNAL OF MATERIALS SCIENCE 32 (1997) 259–266

Shear fracture mechanism in a rapidly-solidified aluminium scrap alloy

D. M. LI*, A. BAKKER
Department of Materials Science, Delft University of Technology, Rotterdamseweg 137, 2628 AL Delft, The Netherlands.

The shear fracture mechanism in a rapidly-solidified aluminium alloy was investigated using both smooth and circumferentially-notched bars under uniaxial tension in a temperature range of 193–423 K and a strain rate range of 10^{-5}–1 s^{-1} for the alloy under as-extruded and precipitation-hardened states. An analytical procedure was performed to make corrections on the hydrostatic stresses in the necked region of a smooth specimen. A complete shear fracture occurs only for the as-extruded alloy in plain tension at intermediate temperatures and relatively low strain rates. The interfacial delamination is associated with both the gross shear fracture in plain tension and the local shearing in notch tension. Based on experimental observations combined with analytical results, a constraint-releasing mechanism is proposed which fairly accounts for the conditions under which the present shear fracture is evident.

1. Introduction

Under a plain tensile condition, fracture by sliding along a definite shear band is evidenced as a typical failure mode of single crystals. For polycrystalline metals, it has been recognized that a similar fracture process by exclusive shearing (*i.e.* with its path $\sim 45^\circ$ to tensile axis) is also possible provided that the purity of the alloy is high enough to prevent micro-void initiation. In the case of commercial alloys this pure shear fracture is usually characteristic of the failure mode of a thin sheet, *i.e.* under plane stress loading conditions. Nevertheless, the occurrence of this fracture mode has been reported for some commercial alloys (mostly aluminium alloys) in plain tension of round bar specimens [1–5] although the normal fracture mode (with a "cup-cone" appearance) is commonly taken for granted in this case.

For commercial alloys under nominally non-plane-stress conditions, it is still difficult to establish a unified theory to account for the mechanism of shear fracture due to the complexity of the mechanical and metallurgical influences involved. However, this does not preclude some significant contributions to the factors promoting shear fracture. Most analytical contributions tend to be based on the assumption that shear fracture is a process or a consequence of localised or unstable flow [3–6]. In an early theoretical model [6], a critical strain is proposed above which flow instability is initiated. It is predicted by this model that the susceptibility of a material to the unstable flow increases with decreasing strain-hardening rate or strain rate sensitivity or stiffness of the test device and with increasing strain rate or the material's specific heat. Amongst these factors the specific heat of the material reflects a thermal softening effect which affects the flow localization by inducing an adiabatic deformation, with the softening effect enhanced at low temperatures or high strain rates [7, 8]. The other factors reflect mechanical softening effects. Later Chung *et al.* [3] proposed a criterion for the flow localization from a viewpoint of the negative free energy requirement. The outcome of this criterion is basically the same as that predicted by the previous model [6]. By neglecting such items as adiabatic heating, Chung *et al.* [3] suggest that a negative strain rate sensitivity of the flow stress (strain rate softening) and/or a negative strain-hardening rate (strain softening) is required for the occurrence of flow localization. The problem lies in that these models do not provide adequate information specific to shear fracture, since unstable deformation or plastic instability actually includes processes other than shear fracture, such as the necking process, while the serrated flow behaviour also belongs to flow localization. For instance, as the serrated flow behaviour has been identified to be associated with the negative strain rate sensitivity [3, 4, 9, 10], it seems impossible to set a criterion on the basis of this sensitivity. More recently Chen *et al.* [5, 11] extend the criterion for shear localization in single crystals [12, 13], namely, that the ratio of the slip plane strain-hardening rate to the current tensile stress reaches a critical value, to predict the macroscopic shear localization in polycrystalline commercial Al alloys. However, the validity for this extension is not verified in their study [5] except that the value of the critical ratio at fracture is evaluated according to the fracture mode. It appears that more systematic investigations need to be carried out to understand the

* *Present address*: Department of Materials Science & Engineering, Pohang University of Science & Technology, Pohang 790-784, Korea.

0022–2461

mechanism of shear fracture under the specified condition.

While recycling aluminium alloys from their scrap has great importance in energy-saving, conventional recycling techniques can not provide the recycled alloys with satisfactory properties, especially toughness [14]. Rapid solidification processing (RSP) has been adopted in recent years as a novel technique for Al scrap recycling purposes because it results in a refined microstructure and hence, improved performance of the alloys. However, little is known about the shear fracture behaviour in the rapidly-solidified (RS) aluminium alloys. The present study is conducted for the purpose of investigating the mechanism of shear fracture in an RS Al scrap alloy.

2. Experimental procedure

The material used for this study was an aluminium scrap alloy. It had a nominal chemical composition of, in weight percent, 7.0 Si, 2.7 Cu, 1.5 Zn, 1.1 Fe, 0.3 Mn, 0.3 Mg, 0.1 Cr, 0.1 Ni, 0.04 Ti, and balance Al. The alloy was received in the form of recycled pilot units extruded in an industrial scrap processing plant in the Netherlands. Before extrusion the alloy was solidified using an RSP technique called melt spinning which is a key process for the recycling of Al scrap. Following the melt spinning process, the melt was directed onto a copper wheel, spinning at a high speed, to provide a cooling rate of about 10^6 K s^{-1}, yielding thin ribbons. Then these ribbons were chopped into flakes and compacted into preforms for the convenience of further forming. The extrusion was performed at a temperature of approximately 723 K with an extrusion ratio of 33:1. From these extruded units both smooth round bar and circumferentially-notched round bar specimens were machined for tensile tests, with their longitudinal (tensile) axes in the extrusion direction. The smooth specimen had a diameter of 8 mm and a gauge length of 40 mm. The notched specimen had a gross diameter of 10 mm for a gauge length of 100 mm. The notch was of a 60° V-type and circumferentially cut at the centre of gauge length, with a depth of 2 mm and a root radius of 0.25 mm. Another batch of specimens were heat-treated before tensile testing. They were heated to 723 K and held for 15 min, quenched in water, and aged at 423 K for 24 h, reaching a peak hardness. All tensile tests were performed in an Instron 4505 testing machine equipped with a data-processing computer system. For the smooth specimens, the tests were conducted at different temperatures ranging from 193–423 K and an apparent strain rate range of 10^{-5}–1 s^{-1}. The notched specimens were only pulled at room temperature and a cross-head speed of 2 mm min^{-1}. The contour of the necked volume was measured for each smooth specimen using a microscopic ruler. Observations under both an optical microscope and a scanning electron microscope (SEM) were made to examine metallurgical and fractographic details.

3. Results

3.1. Plain tensile test results

3.1.1. Temperature and strain rate dependence of mechanical behaviour.

In the temperature and strain rate ranges considered, the as-extruded (AE) alloy exhibits two trends of strain rate sensitivity of flow stress: positive (an increase in the stress–strain envelope with increasing strain rate) and negative (a decrease in the stress–strain envelope with increasing strain rate). At temperatures higher than 353 K, the AE alloy exhibits positive sensitivity. At temperatures between 333–353 K, the sensitivity remains positive in the low strain rate range but turns negative in the high strain rate range. In the temperature range of 293–313 K, the sensitivity stays negative over the whole strain rate range involved. Then, as the temperature decreases, the sensitivity is negative only at low strain rates, as is the case for 233 K. At temperatures lower than 233 K, the sensitivity turns back to a positive value. Fig. 1* shows the yield strength (YS) and the ultimate tensile strength (UTS) as functions of strain rate for typical temperatures at which an obvious transition in the sensitivity is clearly seen. The heat-treated (HT) alloy exhibits a positive sensitivity independent of temperature or strain rate range.

At a definite strain rate, the gross trend for the temperature dependence of strength is that both YS and UTS decrease with increasing temperature. However, it should be noted that in the intermediate temperature range these strength parameters stay almost constant, or rather, show an insignificant peak, as is shown in Fig. 2. For the HT alloy, YS and UTS monotonically decrease with increasing temperature as is typical of many precipitation-hardened alloys. For this group the range of YS and UTS values measured at different temperatures and strain rates are 270–320 MPa and 380–450 MPa respectively.

The true stress (σ)–true strain (ε) data obtained in the present tensile tests follow the Holloman equation $\sigma = K\varepsilon^n$ for the homogeneous deformation stage, where n is the strain-hardening exponent and K is the characteristic stress constant. It is found that the values of n and K account for the trend of flow stress: an increase in flow stress corresponds to an increase in both n and K, and *vice versa*. After heat-treatment both n and K decrease although the flow stress level is greatly elevated. The values of n vary with temperature and strain rate in the range of 0.15–0.23 for the AE alloy and 0.10–0.14 for the HT alloy respectively.

For the AE alloy, the reduction of area (RA) generally decreases with increasing strain rate. However, at temperatures between 293–313 K, this decreasing tendency is replaced by a stable shelf in the intermediate strain rate range, as is shown in Fig. 3. As expected, the true fracture strain (TFS), which is expressed by $\ln(A_o/A_f)$ with A_o and A_f as the initial and the final (at neck) cross-sectional areas respectively, changes in the same trend as RA. For the HT alloy RA and TFS decrease with increasing strain rate in a monotonic manner for all temperatures considered. For both AE

*All figures refer to results for the as-extruded (AE) state except otherwise noted.

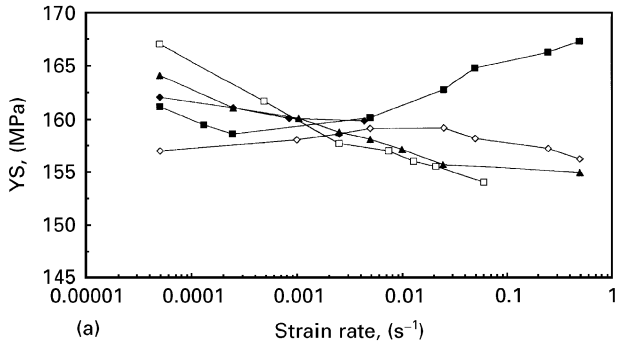

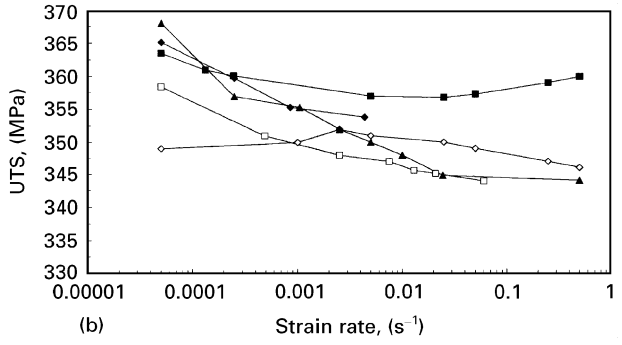

Figure 1 Variation of yield strength (YS) (a) and ultimate tensile strength (UTS) (b) with strain rate in plain tension at a series of temperatures represented by: (◇) 333 K, (□) 313 K, (▲) 293 K (◆) 263 K and (■) 233 K.

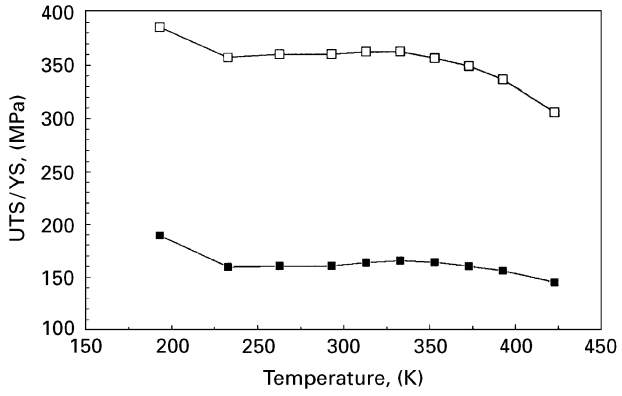

Figure 2 Yield strength ((■) YS) and ultimate tensile strength ((□) UTS) as functions of temperature at a constant strain rate of $2.5 \times 10^{-3}\,s^{-1}$.

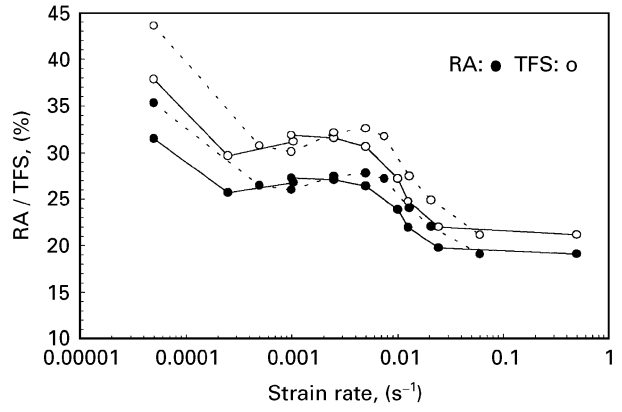

Figure 3 Strain rate dependence of reduction of area ((●) RA) and true fracture strain ((○) TFS) at temperatures of: (—) 293 K and (– – –) 313 K.

and HT alloys tested at a definite strain rate, RA and TFS increase with increasing temperature in general, but with a stable shelf in the intermediate temperature range for the AE alloy, as is indicated in Fig. 4. For the HT group RA varies with temperature and strain rate in a range of 9–13%.

3.1.2. Fractographic observations

For the HT alloy tested in the present temperature and strain rate range, all specimens are broken in a normal fracture mode with a "cup-cone" fracture surface. The proportion of flat fracture area increases with decreasing temperature. For the AE group, when the temperature is higher than 353 K or lower than 233 K, the fracture is also of a normal mode. A typical shear fracture is only found in the temperature range between 233–353 K for specific strain rates detailed in the forthcoming section. Fig. 5 gives an example of the

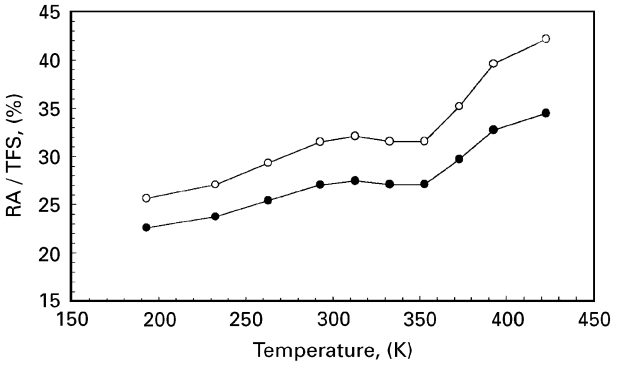

Figure 4 Reduction of area ((●) RA) and true fracture strain ((○) TFS) as functions of temperature at a constant strain rate of $2.5 \times 10^{-3}\,s^{-1}$.

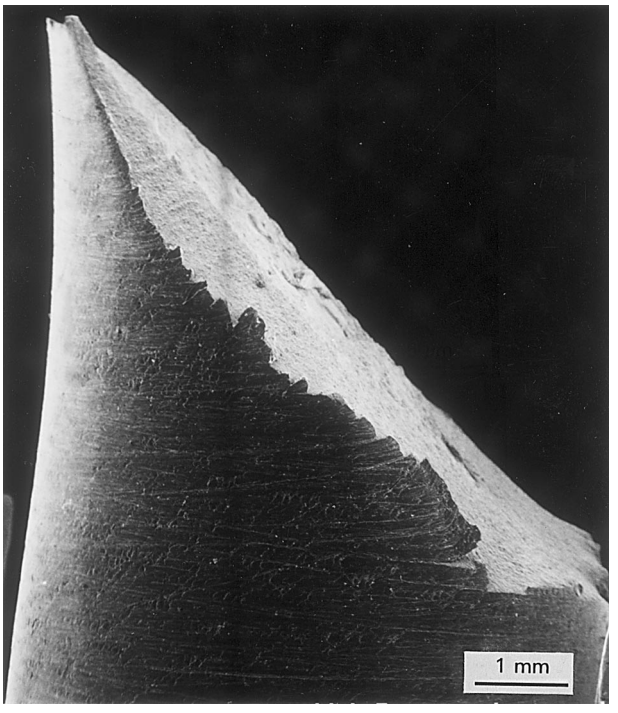

Figure 5 Fracture contour of a specimen broken in plain tension at a temperature of 293 K and a strain rate of $5 \times 10^{-3}\,s^{-1}$ (by SEM, with tensile axis vertical), characteristic of all the specimens broken in a shear fracture mode.

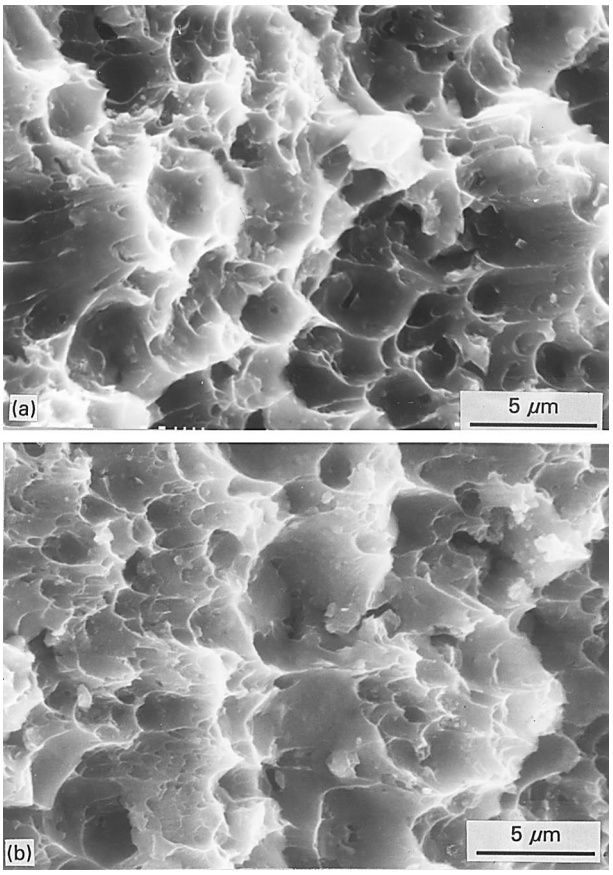

Figure 6 (a) SEM fractographs (45° tilt) showing a typical shear fracture surface and (b) the shear-lip area of a normal "cup-cone" fracture surface (HT specimen) in plain tension (tensile axis horizontal.

shear fracture contour. The micro-mechanism of the shear fracture is micro-void coalescence evidenced by the dimple pattern on the fracture surface, with the difference from the normal fracture appearance only in the dimple shape: the stretched dimples being characteristic of the shear fracture (Fig. 6a). This dimple pattern is basically the same as the one found in the shear-lip area of a "cup-one" fracture (Fig. 6b).

On the fracture surface of a specimen broken in a complete shear mode, the typical dimple pattern (as in Fig. 6a) is interrupted in the central area by a region where some secondary cracks are evidenced (Fig. 7a). With tilting the surface at an angle of $\sim 45^{\circ}$, the crack-forming interface has an appearance characteristic of interfacial debonding or delamination (Fig. 7b). By sectioning the necked area of a specimen unloaded just before fracture, micro-cracks are frequently found in the longitudinal orientation, as is shown in Fig. 7c. These features are characteristic of the AE alloy and they are not evidenced in the HT alloy.

3.1.3. Stress analysis for necked region

With the evidence of interfacial delamination found in the necked region, it seems necessary to evaluate the stress state for that region. For this purpose a correction on the hydrostatic stress should be made. Bridgeman [15] originated this correction work several decades ago by establishing both the constitutive relations and experimental data base obtained from

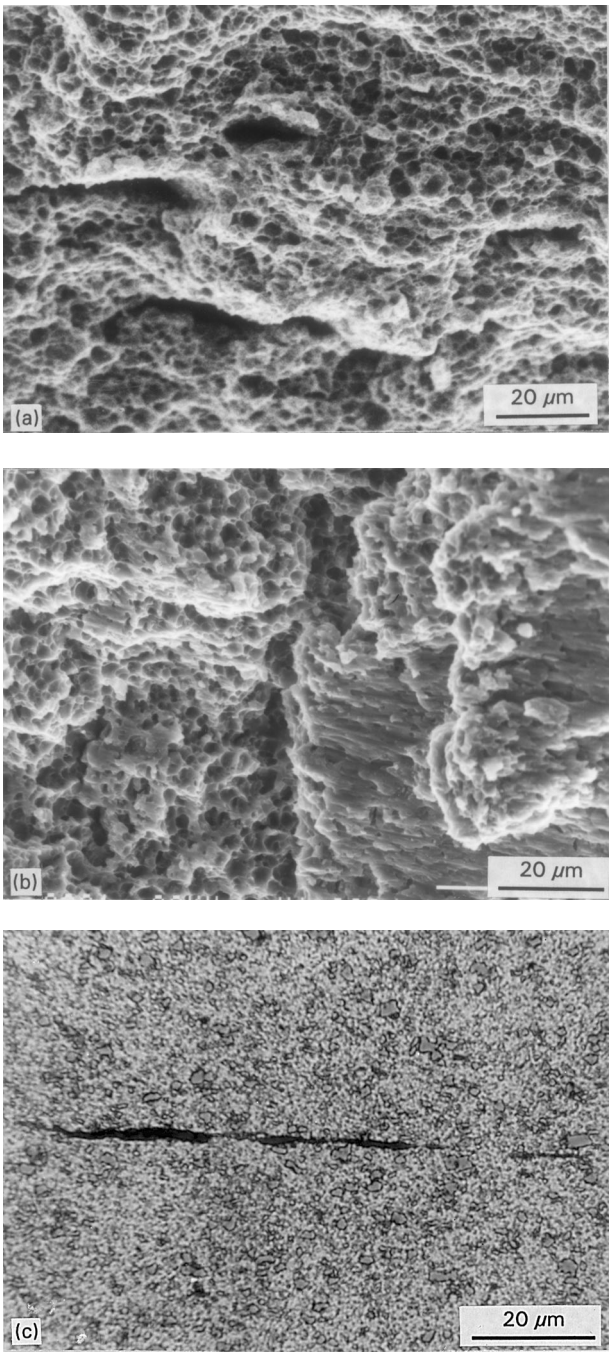

Figure 7 SEM fractographs showing (a) secondary cracks formed by interfacial delamination in the central area of fracture surface (no tilt), (b) features of the delaminated area (45° tilt) and (c) optical metallurgraphic profile showing micro-cracks in the necked region, with tensile axis vertical for (a) but horizontal for (b) and (c).

a series of alloys. Little progress has been found regarding this correction in subsequent decades. Rather, emphasis has been put on the criterion and the influence on the necking process [16–19]. More recently some calculations using the finite elements method (FEM) have been performed by Bakker [20] to account for the strain-hardening dependence of the stress correction. The results of this study suggest that Bridgeman's correction approaches but underestimates the hydrostatic stress. The present analysis is based on Bridgeman's correction [15] since there is sufficient experimental data obtained under different strain-hardening values.

Bridgeman's correction assumes a circular curvature for the neck contour and requires experimental data of the relative neck curvature a/R (a = specimen radius at neck, R = radius of neck curvature) to calculate the hydrostatic stresses. This assumption has been examined in the present study by regressing different sets of a data measured in the neighbourhood of the neck. The results indicate that the standard error for R is 0.002–0.003 mm, which is smaller than the error in measuring a (0.005 mm), revealing good precision in the approximation by Bridgeman's assumption. Experimental data of a/R are plotted against the true plastic strain at the neck (true fracture strain for the present case) as shown in Fig. 8a. These data fall on the upper bound of previous experimental data of a/R collected on a series of alloys including steels, bronzes and brasses [15]. Since a/R reflects geometrically the degree of strain concentration around the necked region, the high a/R value for a definite strain implies that the flow localization is a protruding issue for the alloy used. With the a/R data provided, the ratio of flow stress (σ_f) to the mean axial stress (σ_{ax}), commonly called the correction factor (CF), can be calculated according to [15]

$$CF = \sigma_f/\sigma_{ax} = 1/(1 + 2R/a)/\ln[1 + a/(2R)] \quad (1)$$

The values of CF are also plotted against the true plastic strain at neck as is shown in Fig. 8b.

With the data of the mean axial stress $\sigma_{ax}(= P/\pi a^2$ where P is the tensile load) at fracture, the corrected fracture stress σ_F can be obtained by calculating σ_f at fracture using Equation 1. Fig. 9a gives a map of σ_F values for all specimens fractured by a pure shear mode at different temperatures and strain rates. These σ_F values fall into a narrow range of 351–372 MPa. Then the two transverse stress components, namely, the radial stress σ_{rr} and the circumferential stress $\sigma_{\theta\theta}$, can be estimated following the relation:

$$\sigma_{rr} = \sigma_{\theta\theta} = \sigma_f \ln[1 + a/(2R) - r^2/(2aR)] \quad (2)$$

where r represents the radial coordinate originating at the central point of the cross-section. The values of σ_{rr} at fracture for $r = 0$ are given in Fig. 9b for all specimens of the pure shear fracture family. Similarly, the σ_{rr} ($r = 0$) values also fall within a narrow range of 52–64 MPa. The σ_F and σ_{rr} ($r = 0$) values for the smooth specimens other than the shear fracture family are generally lower than the range indicated above.

3.2. Notch tensile test results

The notch tensile test is aimed to confirm the susceptibility of the alloy to interfacial delamination since this test is advantageous over the plain tensile test in that the constraint is intensified by introducing a stress concentrator like a notch. For the AE alloy the macroscopic fracture surface is perpendicular to the tensile axis i.e. a flat fracture surface. However, on the fracture surface, the appearance of delamination is clearly evidenced, especially as is shown on the profile of

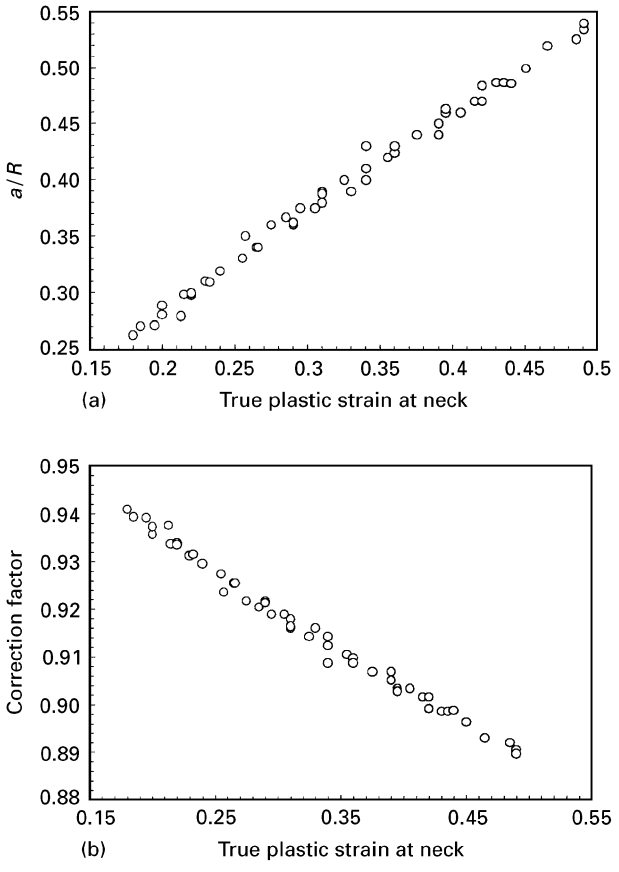

Figure 8 (a) Relative neck contour curvature a/R and (b) Bridgeman's correction factor CF as functions of true plastic strain at neck.

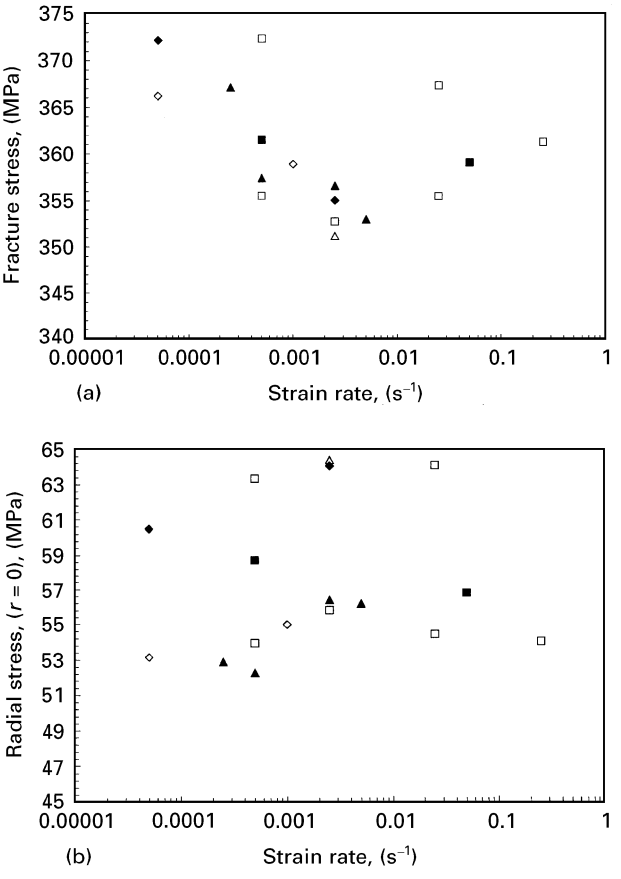

Figure 9 (a) Corrected fracture stress and (b) radial stress at fracture at cross-sectional centre ($r = 0$) for all specimens fractured by a pure shear mode in plain tension under specific temperature and strain rate conditions. The temperatures used were; (△) 353 K, (◇) 333 K, (□) 313 K, (▲) 293 K, (◆) 263 K and (■) 233 K.

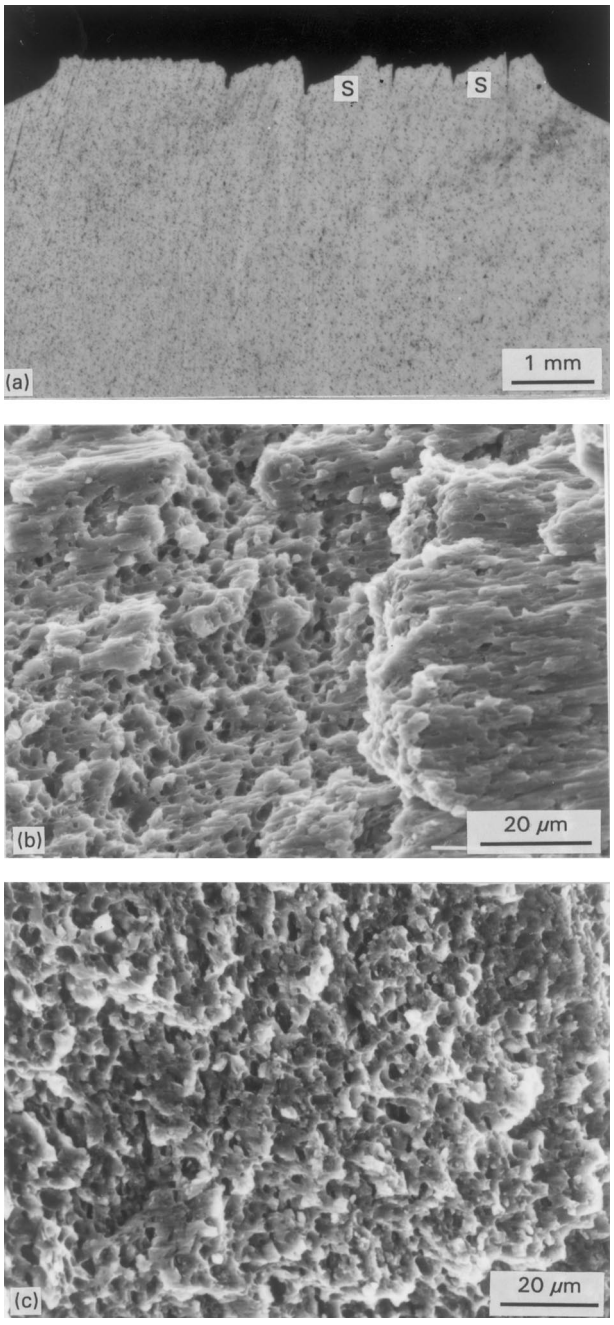

Figure 10 (a) Metallurgical profile of the notched specimen longitudinally-sectioned after fracture and (b) SEM fractographs showing details of delaminated interfaces and (c) appearance of local slant fracture surface ($\sim 45^\circ$ tilt) as is marked in (a) by "S", with tensile axis vertical for (a) but horizontal for (b) and (c).

a longitudinally-sectioned specimen (Fig. 10a). By comparing Fig. 10b with Fig. 7b, it is clear that the delaminated interfaces have an appearance much like that found in the smooth tensile specimens. The local slant fracture area is evident between delaminations, as is shown in Fig. 10a. These slant surfaces are characterized by stretched dimples and ridges (Fig. 10c), implying a shearing process. For the HT alloy the extent of delamination is greatly decreased regarding both the density and the magnitude.

4. Discussion

As was stated earlier, strain softening, strain rate softening and thermal (adiabatic) softening are amongst the main mechanisms promoting shear fracture in commercial alloys. In the present case, shear fracture occurs in the AE alloy but not in the HT alloy while the strain hardening exponent is higher in the former than in the latter. Even for the AE alloy shear fracture is evident in a temperature range where a peak of the strain hardening exponent appears. This consequence contradicts the conventional argument that a low strain hardening rate should facilitate shear fracture [6]. The negative strain rate sensitivity is usually thought to be a criterion for initiating shear fracture [3–4]. In the present study, despite that for the majority of specimens shear fracture occurs under the condition of the negative strain rate sensitivity, there are still certain specimens with the occurrence under the condition of the positive sensitivity, as is the case at temperatures of 233, 333 and 353 K (Fig. 9 and Fig. 1). It seems that the negative sensitivity requirement is not a necessity for shear fracture as it is for serrated flow [3, 4, 9, 10]. For the adiabatic effect, a decrease in temperature or an increase in strain rate is generally considered to enhance the susceptibility to the flow localisation and hence, to shear fracture [3, 7, 8]. In the present case, however, shear fracture does not occur when the temperature is lower than 233 K. In the temperature range where shear fracture is evident, the occurrence is dominant at relatively low strain rates. This means that the adiabatic effect is not a direct mechanism inducing the present shear fracture. In view of the present experimental results, it is important to note that there is basically no difference between micro-mechanisms of the shear fracture and the normal "cup-cone" fracture: since both occur by a process of micro-void coalescence characterized by the dimple pattern. The difference is reflected only in the dimple shapes, i.e. with stretched dimples being characteristic of shear fracture (Fig. 6a) whilst equiaxed dimples are characteristic for the normal (flat) fracture surface. However, even this stretched dimple pattern is identical to the one found in the shear-lip part of a "cup-cone" fracture surface (Fig. 6b). Therefore the present fracture behaviour is dominated by fracture macro-mechanism or fracture mode transition (plane strain/normal versus plane stress/shear) instead of fracture micro-mechanism transition (micro-void coalescence versus cleavage versus intergranular degrading). Then the constraint effect should be taken into consideration.

One important manifestation characteristic of the present fractographic observations is the delamination phenomenon which is intensified through the triaxial loading in notch tensile tests (Fig. 10). This phenomenon has been reported in recent years both for conventionally-solidified aluminium alloys [21, 23] and for rapidly-solidified alloys [24]. One characteristic common to these alloys is that there exists a certain type of weak boundary or interface, either the boundary of the mechanically-elongated or flattened grain [21, 23] or the interface of prior powder particle [24]. The weak boundary causing the present delamination is judged to be the interface of prior ribbon flakes which tend to take a longitudinal orientation due to extrusion force. As is shown in

Fig. 10, local-scale shear fracture occurs in the ligaments between delaminated interfaces. In fact, these ligaments act as individual thin sheets under a loading condition approaching a plane stress state, because the constraint in the neighbourhood is released considerably due to the delaminations. It is interesting to note the dual effects resulted from the interaction between the mechanical variant (stress triaxiality introduced by notch) and the metallurgical variant (weak interface). The triaxiality should normally promote plane strain fracture (flat fracture). However, when there exist weak interfaces this same triaxiality can also promote plane stress fracture (shear fracture) due to delamination of the interfaces under the action of transverse stress components, as is the present case. Therefore it can be concluded that the local shear fracture (or local shearing) is promoted by a constraint-releasing mechanism.

The delamination also occurs in the smooth tensile specimens of the AE alloy (Fig. 7) although the extent of the delamination is moderated appreciably compared with the notch tension case. It is worthwhile to note that the shear fracture is evident under the condition that the necking process has developed considerably as is indicated by the magnitude of the relative neck curvature a/R. Then it is reasonable to assume the existence of a triaxiality state (or hydrostatic state) and hence, the existence of transverse stresses. The correction on the hydrostatic stresses results in a radial (or circumferential) stress range of 52–64 MPa. Yet it is difficult to conduct a direct measurement of the interface bonding strength for the present material due to the cylindrical distribution of the prior flakes. Nevertheless, the interfacial debonding for some aluminium-based composites has been reported to occur under a stress level ranging from 10–50 MPa [25–27]. This can serve as a reference, suggesting that the interfacial bonding strength can be very low and that it is fairly possible for the present delamination to happen under the action of the transverse stress. More important is the experimental observation that the shear fracture in the present condition is always associated with the occurrence of delamination. Consequently the constraint-releasing mechanism is also assumed for the shear fracture in smooth tensile bars as is for the local shearing in notched tensile bars. For the plain tensile case, however, only the central region of the specimen is required to apply this mechanism since the circumferential region is intrinsically in a plane stress state. With this mechanism, the propensity of the alloy to shear fracture can be clarified in response to temperature and strain rate variation. For the weak interface to delaminate under the action of transverse stresses, a high flow stress combined with a high value of a/R is required at the moment of fracture, according to Equation 2. In the intermediate temperature range especially at temperatures between 293–313 K, both flow strength and a/R maintain adequate values to yield a high value of σ_{rr} or $\sigma_{\theta\theta}$. That is why most members of the shear fracture family are located in this intermediate temperature range (Fig. 9). At high temperatures (e.g. > 353 K), the a/R value is rather high due to an increase in RA, but flow stress at fracture (σ_F) is low. At low temperatures (e.g. < 233 K), σ_F and a/R exchange their trends. In both cases, the resultant transverse stress level is not sufficient for the delamination to occur. It should be pointed out that the present shear fracture family only includes those members (specimens) whose fracture is a pure (or complete) shear mode; the constraint-releasing mechanism should also facilitate incomplete shear fracture (i.e. with an insignificant portion of normal fracture). Attention should also be paid to the point that the requirement on the transverse stress level is necessary (for delamination) but not sufficient criterion for the occurrence of shear fracture in the present condition. There are exceptions where the metallurgical imperfections cause the early initiation of a central crack, producing a normal fracture portion in the central region. That is why only a few members qualify for the shear fracture family even in the intermediate temperature range.

5. Summary

Under the present test conditions, a complete (or pure) shear fracture is found only in plain tension of the as-extruded alloy at intermediate temperatures and relatively low strain rates. Strain rate softening and adiabatic softening mechanisms do not seem to contribute directly to the occurrence of shear fracture. One important experimental observation is that the shear fracture is always associated with interfacial delamination which is intensified in the notch tensile test. The analysis of the hydrostatic stress correction confirms the existence of two transverse stress components with a magnitude in the range of 52–64 MPa (in the specimen centre), higher than those calculated for the specimens with a normal fracture. Then a constraint-releasing mechanism is considered responsible for the present shear fracture. The heat-treatment apparently improves the interfacial bonding in addition to the precipitation-hardening effect. Correspondingly, there is no complete shear fracture evident in the heat-treated alloy.

Acknowledgement

The present work was made possible by Dr W. H. Kool kindly providing the samples and by the financial support of the Research Fellowships Commission, Delft University of Technology.

References

1. D. A. RYDER and A. C. SMALE, "Fracture of Solids" edited by D. C. Drucker and J. J. Gilman (Interscience Publishers, 1963) p. 237.
2. P. J. E. FORSYTH and A. C. SMALE, *Eng. Fract. Mech.* **3** (1977) 127.
3. N. CHUNG, J. D. EMBURY, J. D. EVENSEN, R. G. HOAGLAND and C. M. SARGENT, *Acta Metall. Mater* **25** (1977) 377.
4. J. E. KING, C. P. YOU and J. F. KNOTT, *Ibid.* **29** (1981) 1553.

5. C. Q. CHEN and H. X. LI, *Mater. Sci. & Tech.* **3** (1987) 125.
6. W. A. BACKOFEN, "Fracture of Engineering Materials" (ASM, Ohio, 1964) p. 118.
7. A. U. SULIJOADIKUSUMO and O. W. DILLON, JR. "Metallurgical Effects in High Strain Rates" edited by R. W. Rohde *et al.*) (Plenum Press, New York, 1973), p. 501.
8. R. S. CULVER, *ibid.* p 519.
9. P. PENNING, *Acta Metall. Mater.* **20** (1972) 1169.
10. J. C. HUANG and G. T. GRAY, *Scripta Metall. Mater.* **24** (1990) 85.
11. C. Q. CHEN, in: Proc. ICF Int. Symp. on Fracture Mechanics edited by K. C. Hwang *et al.* (Science Press, Beijing, 1983) 871.
12. R. J. ASARO, *Acta Metall. Mater.* **27** (1979) 445.
13. D. PEIRCE, R. J. ASARO and A. NEEDLEMAN, *ibid.* **30** (1982) 1087.
14. J. MOERMAN, H. KLEINJAN and W. H. KOOL, in: Proc. Int. Conf. on the Recycling of Metals, edited by B. Cina (ASM European Office, Brussels, 1992) p. 127.
15. P. W. BRIDGEMAN, "Studies in Large Plastic Flow and Fracture" (McGraw-Hill, New York, 1952).
16. J. J. JONAS, R. A. HOLT and C. E. COLEMAN, *Acta Metall. Mater.* **24** (1976) 911.
17. J. W. HUTCHINSON and K. W. MEALE, *ibid.* **25** (1977) 839.
18. A. K. GHOSH, *ibid.* **25** (1977) 1413.
19. F. A. NICHOLS, *ibid.* **28** (1980) 663.
20. A. BAKKER, in Proceedings of the Fifth International Conference on Numerical Methods in Fracture Mechanics, Freiburg, FRG, April 1990, edited by A. R. Luxmoore and D. R. J. Owen (Pineridge Press, Swansea, UK) p. 433.
21. R. C. DORWARD, *Scripta Metall.* **20** (1986) 1397.
22. K. T. VENKATESWARA RAO, W. YU and R. O. RITCHIE, *Metall. Trans.* **20A** (1989) 485.
23. K. T. VENKATESWARA RAO and R. O. RICHIE, *Acta Metall. Mater.* **38** (1990) 309.
24. W. C. PORR, JR. and R. P. GANGLOFF, *Metall. Mater. Trans.* **25A** (1994) 365.
25. T. ERTURK, J. A. CORNIE and R. G. DIXON, in: "Interfaces in Metal–Matrix Composites" edited by A. K. Dhingra and S. G. Fishman (The Metallurgical Society, Inc. 1986) p. 239.
26. B. Z. JANG, L. R. HWANG and Y. K. LIEU, *ibid.* P. 95.
27. K. HASHIMOTO, S. SEKIGUCHI and K. YAMADA, in: "Interfaces in Metal–Ceramic Composites" edited by R. Y. Lin *et al.* (TMS 1990) p. 551.

Received 15 April 1994
and accepted 15 December 1995